Title	Optical properties of c-Plane InGaN/GaN single quantum wells as a function of total electric field strength
Authors	Christian, George M.;Schulz, Stefan;Hammersley, Simon;Kappers, Menno J.;Frentrup, Martin;Humphreys, Colin J.;Oliver, Rachel A.;Dawson, Philip
Publication date	2019-04-23
Original Citation	Christian, G. M., Schulz, S., Hammersley, S., Kappers, M. J., Frentrup, M., Humphreys, C. J., Oliver, R. A. and Dawson, P. (2019) 'Optical properties of c-Plane InGaN/GaN single quantum wells as a function of total electric field strength', Japanese Journal of Applied Physics, 58, SCCB09 (7pp). doi: 10.7567/1347-4065/ab0407
Type of publication	Article (peer-reviewed)
Link to publisher's version	http://dx.doi.org/10.7567/1347-4065/ab0407 - 10.7567/1347-4065/ab0407https://data.mendeley.com/datasets/5c9b7283td/1
Rights	© 2019, The Japan Society of Applied Physics. Published by IOP Publishing. This Accepted Manuscript is available for reuse under a CC BY-NC-ND 3.0 licence after the 12 month embargo period provided that all the terms of the licence are adhered to. - https://creativecommons.org/licenses/by-nc-nd/3.0/
Download date	2025-07-31 17:07:29
Item downloaded from	https://hdl.handle.net/10468/9531

Optical properties of *c*-Plane InGaN/GaN single quantum wells as a function of total electric field strength

George M. Christian[1*], Stefan Schulz[2], Simon Hammersley[1,3], Menno J. Kappers[4], Martin Frentrup[4], Colin J. Humphreys[4,5], Rachel A. Oliver[4], and Philip Dawson[1]

[1]*School of Physics and Astronomy, Photon Science Institute, University of Manchester, Manchester, M13 9PL, UK*

[2]*Photonics Theory Group, Tyndall National Institute, University College Cork, Cork, T12 R5CP, Ireland*

[3]*School of Electrical and Electronic Engineering, University of Manchester, Manchester, M13 9PL, UK*

[4]*Department of Materials Science and Metallurgy, 27 Charles Babbage Road, University of Cambridge, Cambridge, CB3 0FS, UK*

[5]*School of Engineering and Materials Science, Queen Mary University of London, London, E1 4NS, UK*

[*]E-mail: george.christian@manchester.ac.uk

We present low temperature photoluminescence spectra from four InGaN/GaN single quantum well structures where the total electric field across the quantum wells was varied by the manipulation of the surface polarization field, which is of opposite sign to the electrostatic built-in fields originating from spontaneous and piezoelectric polarization intrinsic to the material. We find that, overall, the photoluminescence peak emission energy increases and its full width at half maximum decreases with decreasing total internal electric field. Using an atomistic tight-binding model of a quantum well with different total internal electric fields, we find that the calculated mean and standard deviation ground state transition energies follow the same trends with field as our experimentally determined spectral peak energies and widths. Overall, we attribute this behavior to a reduction in the quantum confined Stark effect and a connected reduction in the variation of ground state transition energies with decreasing electric field, respectively.

1. Introduction

The built-in electrostatic fields across *c*-plane InGaN/GaN quantum wells (QWs) have been shown to play an important role in their optical properties. For instance, the combination of alloy fluctuations and the built-in field leads to strong carrier localization effects.[1–7] This carrier localization is generally accepted as the reason for the high room temperature internal quantum efficiencies (IQEs) of these structures since it prevents carrier diffusion to non-radiative centers such as dislocations and possibly point defects.[1–11] From a theoretical perspective, we have previously demonstrated[1–3] that holes are strongly localized by random alloy fluctuations and that electrons are localized by a combination of effects due to the built-in electrostatic fields, random alloy fluctuations and well width fluctuations (WWFs). We have also previously shown experimentally[12–15] that the inclusion of a Si-doped, *n*-type InGaN underlayer (UL) in InGaN/GaN QW structures leads to an enhancement of the surface polarization field which acts in the opposite direction to the intrinsic electrostatic built-in fields.[16] This occurs because of the pinning of the Fermi level at the conduction band edge in the region of the *n*-type UL and at the valence band edge at the GaN/air interface due the large charge density formed by the discontinuity in the spontaneous polarization.[17] Overall, this results in a reduction in the total field across the QW(s), giving rise to shorter radiative recombination lifetimes[12–15] and increased room temperature IQEs[12,13] measured for QW structures containing ULs. Although an alternative mechanism for the improvements due to ULs has been proposed whereby point defects or impurities are trapped in the UL, preventing their diffusion into the QWs,[18] other groups have reported[19–21] similar improvements for QW structures where the total electric field has been reduced by modifying the barrier alloy composition and/or doping concentrations, consistent with our previous experimental work. While these improvements are attractive for the development of high efficiency light emitting diodes (LEDs), the effects of the reduced electric field on carrier localization need to be investigated, as our previous work[2] has shown that the variation in (ground state) energies of localized carriers is sensitive to the strength of the electric field across the QW.

In this paper, we report on the low temperature (10 K) photoluminescence (PL) spectra from a series of *c*-plane single QWs across which the total electric field was controlled by varying the total distance between an *n*-type InGaN UL and the sample surface. As the

strength of the surface polarization field is increased by reducing the distance between an n-type layer and the sample/air interface,[17] we can expect that the total electric field across the QWs increases with increasing thickness of the GaN cap layer. We compare our experimentally determined PL peak emission energies and full widths at half maximum (FWHMs) to the average transition energy, and the standard deviation in transition energy, respectively, calculated from 40 different random configurations of a fully atomistic model of an InGaN/GaN QW with a variable external electric field applied in the opposite direction to the intrinsic built-in field. Our results show that modifying the structure of the QW sample can have a similar impact to the application of an external bias on the emission properties.[22]

2. Methods

In this section we provide an overview of the experimental and theoretical methods used to gain insight into the electronic and optical properties of c-plane InGaN/GaN QWs with modified internal built-in fields. In Sect. 2.1 we present details of the design, growth and structural characterization of the samples used for the experimental optical studies. The results of the PL studies are discussed in Sect. 2.2. Our theoretical framework is described in Sect. 2.3.

2.1 Samples

Initially, a range of single QW structures were designed using the commercial device simulator Nextnano3.[23] Following our previous work,[12–15] the structures all contained a Si-doped InGaN UL. The built-in fields across InGaN/GaN QWs resulting from the spontaneous and piezoelectric polarizations are known to be of the order ~-1 MV cm^{-1}.[16,17] The QW composition, well width and barrier width were varied incrementally between our Nextnano3 simulations to arrive at a range of values for these parameters which, in combination, would produce QWs for which the total electric field across the conduction and valence band profiles was reduced by 10-100 times. It is important to note here that the employed model of the InGaN as a uniform, continuous layer is inadequate when describing a real InGaN QW due to local variations in the built-in potential caused by random alloy fluctuations, as we will discuss in detail in introducing our more rigorous theoretical approach below. However, for the purposes of the initial sample design, it is sufficient to study the overall trends in how the average electric field across a QW varies with different

parameters.

Following from our simulations, four single QW structures were grown by metalorganic vapor phase epitaxy on top of 5 μm thick GaN pseudo-substrates with a threading dislocation density of ~4 × 10^8 cm^{-2} deposited on *c*-plane sapphire substrates. For each sample, a 2 μm thick GaN template doped with Si to a density of 6 × 10^{18} cm^{-3} was grown followed by a 24 nm thick $In_{0.059}Ga_{0.941}N$ UL doped with Si to a density of 2 × 10^{19} cm^{-3}. The Si doping densities were confirmed by secondary ion mass spectroscopy measurements. On top of the UL a 3.5 nm thick layer of unintentionally doped GaN was grown followed by a 2.7 nm thick $In_{0.18}Ga_{0.82}N$ QW. Finally, an unintentionally doped GaN cap layer was added. The thickness of the cap layer was varied between the samples to give values of 2.0, 3.0, 4.0 and 5.0 nm, respectively. The cap layer (top QW barrier) thickness was selected as the parameter that could be most effectively controlled to produce a series of QWs where the total electric field varied systematically between them. Nextnano3 simulations of the conduction and valence band edges for the four as-grown samples are shown in Fig. 1. These show that the Fermi level (defined at 0 on the energy scale) is pinned at the conduction band edge by the *n*-type doping in the UL, and at the valence band edge at the sample surface due to the charge density formed by the discontinuity in the spontaneous polarization vector field. According to these simulations, the total electric fields across the 2, 3, 4 and 5 nm cap layer QWs were 0.122, 0.0374, -0.158 and -0.357 MV cm^{-1}, respectively. The electric fields are defined conventionally such that negative fields are in the direction of the piezoelectric polarization field.

The thickness and composition of the individual layers in the single QW structures were confirmed by X-ray diffraction measurements on multi-QW test structures grown under the same conditions.

2.2 Optical measurements

To gain insight into the optical properties of the QW systems, PL measurements were performed under CW excitation using a He-Cd laser with photon energy 3.815 eV and an excitation power density at the sample of 10 W cm^{-2}. The samples were held at 10 K in a closed-cycle He cryostat and inclined at Brewster's angle in the horizontal plane with respect to the collection axis. Only the horizontally polarized component of the PL emission was collected to minimize the impact of Fabry-Pérot interference oscillations on the PL

spectra.[24] Light emitted from the sample was dispersed using a 0.85 m double grating spectrometer and detected using a GaAs photomultiplier tube. The signal was processed using standard lock-in detection techniques.

2.3 Theoretical Framework

To study changes in the electronic and optical properties of c-plane InGaN/GaN QWs in which the intrinsic built-in field is reduced, we proceed as follows. Overall, our theoretical framework builds on a nearest neighbor sp^3 tight-binding model that is discussed in detail in Refs. 1 and 25. This approach allows for an atomistic description of the electronic and optical properties of InGaN/GaN QWs and includes effects such as alloy induced fluctuations in local strain and built-in fields. To achieve, for instance, an atomistic description of random alloy induced (local) variations in the built-in potential, we use our recently developed local polarization theory.[25] This aspect is of particular importance, since when reducing the macroscopic built-in field in a c-plane InGaN/GaN QW, local variations in the field can lead to the situation that the overall macroscopic field is not completely canceled. This is in contrast to the 1-dimensional conduction band simulations described in Sect. 2.1, in which the total field across the 3 nm cap layer QW could be considered negligible in comparison to a QW within a structure without an UL.

Given the atomistic nature of our theoretical framework, all calculations here have been performed on supercells, with periodic boundary conditions, that contain approximately 82,000 atoms. The c-plane InGaN QW width is approximately 3 nm and the In content in the well is set to 15%. These values for In content and well width are in good agreement with the experimentally determined values. Furthermore, we assume a random distribution of In atoms in the well region of the supercell. WWFs at the upper QW interface (GaN on InGaN) have been treated as disk-like objects with a width of approximately 5 nm and a height of 2 monolayers. The assumptions of a random alloy distribution and the presence of WWFs are consistent with previous experimental studies.[26–29]

In general, we are interested in observable trends rather than performing a one-to-one theory-experiment comparison on the impact of a reduced overall electric field. Therefore, in our theoretical framework, we study this question using the In$_{0.15}$Ga$_{0.85}$N/GaN QW discussed above and apply an external electric field over the supercell. This external field

is of opposite sign to the internal electrostatic built-in field arising from spontaneous and piezoelectric polarization, which is obtained from the local polarization theory. For the external field we use a continuum-based description based on the equations given in Ref. 30, for instance. In doing so, we can easily adjust the electric field strength across the $In_{0.15}Ga_{0.85}N$/GaN well from the full built-in field value (no external field) to a value that is close to zero, at least when discussing this in a continuum-based description. This allows us to investigate the cases predicted by the Nextnano3 simulations described in Sect. 2.1, in which the total internal QW field was calculated to be close to zero in the case of the 3 nm cap layer sample and reversed for the 2 nm cap layer sample. As mentioned above, in our fully atomistic picture, the continuum-based description is not necessarily valid since the built-in field might vary locally.

To gain insight into the importance of the underlying microstructure on the results, the calculations have been repeated 40 times. This means we have generated 40 different microscopic configurations (supercells). For each supercell four different external field values have been considered, with cases of an external field (i) that is zero (original system, full internal field), (ii) that approximately halves the internal, spontaneous and piezoelectric polarization related macroscopic built-in field, (iii) that approximately cancels the internal field ("zero" field case) and (iv) that leads to a slight reversal of the combined field (internal plus external field). Again, it should be stressed that this classification is made on the basis of what could be expected from a continuum-based picture. Overall, this leads to 160 electronic structure calculations on supercells each containing approximately 82,000 atoms.

3. Results and discussion

In this section, we present the experimental and theoretical results of our studies. Firstly, the results of our PL spectroscopy and time decay experiments are described in Sect. 3.1, and then the findings of our simulations are presented, discussed and compared with experiment in Sect. 3.2.

3.1 PL spectroscopy

PL spectra for each of the samples are shown in Fig. 2. The spectral intensities for each sample are normalized to that at the zero-phonon emission peak at 2.768, 2.762, 2.746 and

2.752 eV for the 2, 3, 4 and 5 nm cap layer samples, respectively. The peaks at 91 ± 1 meV lower than the main emissions are identified as being due to longitudinal optical (LO) phonon-assisted recombination.[24,31] The zero-phonon emission peak energy and FWHM of the main emission lines are shown varying with GaN cap layer thickness in Fig. 3. The FWHM increases monotonically with increasing cap layer thickness. The peak emission energy decreases by approximately 22 meV as the cap layer thickness is increased from 2-4 nm, and then increases by approximately 6 meV between the 4 and 5 nm cap layer samples. Based on our previous studies of the effects of n-type ULs on the total electric fields across QWs,[13,14] and as well as our simple band-edge profile simulations described in Sect. 2.1, we expect that the total electric field across the QW in each sample decreases with decreasing total distance between the UL and the sample/air interface, i.e. decreasing cap layer thickness.

Without any detailed analysis, the decreasing FWHM with decreasing total electric field across the QW is in agreement with Ref. 2, where the variation in electron ground state energies was found to be sensitive to the strength of the electric field parallel to the growth axis. The effects of varying the total electric field across a QW are examined in detail through our simulations as described in Sect. 3.2. We observed no systematic blueshift of the peak emission energy as the excitation power density was increased by more than 2 orders of magnitude. Therefore we can rule out any contribution to the peak energy and FWHM from state-filling effects. The absolute PL intensity at 10 K did not vary systematically with cap layer thickness between the samples, which suggests that surface states do not play a significant role at 10 K.

Nonexponential PL decay transients (not shown), on timescales of several 10s of ns, were detected at energies across the emission peaks for all of the samples. Such decay curves have previously been reported[6,32] and ascribed to the combined effects of the electric field perpendicular to the plane of the wells and the in plane localization of electrons and holes with varying separations.[6,32] This is radically different from the case on nonpolar InGaN QWs where the absence of the electric field leads to exponential decays on sub-nanosecond time scales involving localized excitons.[32-34] Thus the dynamic behavior of the recombination in the samples studied here suggests that, despite the

predictions of the Nextnano3 calculations, local electric fields continue to play a role in the recombination.

3.2 Atomistic simulation results and comparison to experiment

The main aim of our theoretical study is to establish how electronic and optical properties of c-plane InGaN/GaN QWs change as a function of the total (internal plus external) electrostatic field. Before turning to the electronic structure and the optical properties of our theory model system, we start with an analysis of the electrostatic built-in field.

Figure 4 displays the total electrostatic potential of an arbitrarily chosen microscopic configuration for a slice through the simulation supercell in the x-z-plane when varying the y-coordinate. The z-axis here is always parallel to the wurtzite c-axis. The upper row of Fig. 4 (a) (Full Internal Field) depicts the situation when no external field is present, thus the system is dominated by the intrinsic built-in field due to spontaneous and piezoelectric polarization vector fields. The middle row, Fig. 4 (b) (Reduced Internal Field), corresponds to the situation where, on a continuum-based level, the field is approximately halved compared to the system without any external field (Full Internal Field). The lower row, Fig. 4 (c), shows the data when, again from a continuum-based viewpoint, without any alloy disorder induced effects, the total field should be zero ("Zero" Internal Field). Thus, the internal and external fields should cancel each other exactly for the latter "zero" field system. Please note the different scales used in the different rows. To distinguish the different situations clearly, different colormaps have been used. We start our analysis here by looking at the system when no external field is applied (Fig. 4 (a)). We observe that the potential isolines are not parallel to each other and that depending on the slice taken, the built-in field varies between different slices through the supercell. Also, not shown here, the local variations in the built-in field, and those at the QW/barrier interface, vary significantly between different configurations. Turning to the reduced built-in field case, Fig. 4 (b), where an external field is now present, basically the same situation is found as in Fig. 4 (a), but the alloy induced internal built-in potential fluctuations become even more clearly visible, including at the QW/barrier interfaces. Overall, this indicates already that when applying an external field to the heterostructure it is impossible to fully eliminate built-in field effects, keeping in mind that the situation changes from one microscopic configuration to another. This is confirmed by the results shown in Fig. 4 (c) ("Zero"

Internal Field), where an external built-in field is applied that in a continuum-based picture should result in the ideal situation of a field-free QW system. Here, we observe large local variations in the built-in field, which can reach values comparable in magnitude to built-in potential values found in the system without an external field (Fig. 4 (a)). Larger changes are observed at the QW/barrier interface, especially in the region of the WWF. So even though the spatial separation of the charge carriers along the growth direction can be eliminated, local fluctuations might still lead to significant spatial separations of electron and hole wave functions. While it is possible that one or more of our experimental QW structures has an internal electric field that has *on average* been reduced to close to zero, our atomistic calculations show that it is very difficult if not impossible to produce a *c*-plane InGaN QW that is built-in field-free. This stems also from the fact that WWFs will vary in size and shape and, given that these exhibit larger surfaces areas orientated along the c-axis, the built-in field will vary significantly around these structural inhomogeneities. This is a significant difference to a nonpolar system, where WWFs, due to their crystallographic orientation, are of secondary importance for the residual built-in field in these structures.

To shed more light on this effect, we have calculated the electron and hole ground states for the 40 different microscopic configurations per external field value assumed here (see above). Following Fig. 4, we have used this arbitrarily chosen configuration to display the single-particle electron and hole ground state charge densities for the three different systems discussed in Fig. 5. This figure depicts isosurface plots of the ground state charge densities for electron and hole in red and blue, respectively. The light and dark surfaces correspond to 20% and 40% of the respective maximum charge densities. The left column, Fig. 5 (a), shows the data in the absence of the external field, the middle column, Fig. 5 (b), the results for the reduced built-in field, and the right column, Fig. 5 (c), the charge densities for the case with the external field present and approximately canceling the internal macroscopic field. Focusing on the results without the external field, we observe here the expected behavior that the internal macroscopic electric field spatially separates electrons and holes along the growth direction. Furthermore, the random alloy fluctuations lead to strong hole wave function localization effects, while the electron wave function is mainly localized by the WWFs. These results are consistent with results previously

reported in the literature. These observations are basically unchanged when approximately halving the internal electrostatic built-in field (Fig. 5 (b)). Thus, even when reducing the field significantly, the electron wave function is still strongly localized by the combined effect of built-in field and WWF. Finally, turning to the results where, in the presence of the external field, Fig. 5 (c), the total internal field should approximately be zero, the hole wave function still exhibits pronounced localization features. This behavior is expected since the hole localization characteristics originate from the underlying random alloy induced effects. However, and in contrast to the situation with the full internal field (no external field; Fig. 5 (a)) or a significantly reduced internal field (Fig. 5 (b)), the hole wave function is no longer localized near the bottom of the well. Looking at the electron charge density, we find even more dramatic changes in the localization characteristics. Here, the electron wave function is no longer localized by the WWF. Additionally, the electron charge density exhibits a far more delocalized nature, with perturbations introduced by the random alloy fluctuations. In general, we observe, independent of the microscopic configuration, that in our "zero" field system, holes are strongly localized by random alloy fluctuations and connected variations in the strain and (local) built-in field while the electron wave functions also show perturbations due to the underlying random alloy but that the impact of the WWF is clearly reduced. All this results in the situation that changes in the single-particle electron and hole ground state energies are reduced in the "zero" field case when compared to the situation where no external field is present. This argument is consistent with the findings reported by Baranowski *et al.*,[22] where local changes in the built-in field for the system with no external field have a much bigger effect on the transition energy when compared to a system with an overall reduced built-in field. Thus, from this analysis one could expect a reduction in the FWHM when reducing the internal field by an external field, consistent with the experimental findings discussed above.

To quantify these results in a way that allows for comparison to our experimental findings, Fig. 6 depicts the calculated average transition energy (for each field value averaged over the 40 different microscopic configurations), along with its standard deviation, as a function of the total electric field across the QW. We use the standard deviation to gain insight into the behavior of the FWHM. This approach is chosen here, since from a theoretical viewpoint, to resolve this feature, one would need to go beyond 40

microscopic configurations to predict the corresponding PL spectrum reliably without introducing artifacts by broadening each PL peak from each of the configurations. However, for our purposes, the standard deviation is sufficient to highlight trends. Several features in Fig. 6 are now of interest for our study. Starting with the average transition energies (blue circles), we observe, by reducing the internal built-in field by the external field, a blue shift in the transition energy. A similar effect is also observed in the experiment when decreasing the built-in field by reducing the cap layer thickness (cf. Fig. 3). In general, one expects such a blue-shift since the quantum confined Stark effect (QCSE) is reduced. Also, we find that when going beyond the "zero" field value (reversing the internal field), the transition energy starts to red-shift, again consistent with the QCSE assuming the field now points in the opposite direction when compared to the field in a "standard" (no external field) InGaN/GaN QW. Turning to the results for standard deviation (red squares), we observe that this quantity decreases with increasing external field. Overall, this behavior is consistent with the above-mentioned effect that the variations in the electron and hole single particle energies are reduced and consequently the FWHM value is expected to be reduced. Overall, the above observed results (reduction of FWHM and blue–shift of transition energy with reduced built-in field) will also hold when excitonic effects are included in the theoretical framework. This stems from the fact that the calculated excitonic transitions energies are also affected by the variations in the single-particle energies, given that these present the starting point for any calculation that accounts for Coulombic effects.

Surprisingly, when starting to reverse the internal field, the standard deviation continues to decrease. This is an interesting effect which might originate from the fact that electrons are now being pushed towards the lower QW interface which does not exhibit WWFs on the scale of the upper QW barrier interface.[35] Thus WWFs are no longer important for the electron wave functions. Additionally, for the holes, the dimensions of the WWF are much larger than the localization length. Therefore, one would expect that the macroscopic features of the WWFs are of secondary importance for the hole (ground) states. Further studies are required to shed more light on this observation, which is beyond the scope of the present work. Experimentally for the 2 nm cap layer sample, which exhibits the narrowest FWHM, no red-shift in the peak emission energy is observed

relative to the 3 nm cap layer sample. Therefore, it is unlikely that the internal field has been reversed in this QW structure. The reason for the red-shift in the emission when the cap layer is reduced from 5 to 4 nm is currently unclear.

Overall, we can conclude from our theoretical study that when decreasing the internal field, a reduction in the FWHM value is expected. This decrease in the FWHM with decreasing built-in field should be accompanied by a blue shift in the PL peak energy, unless the field inside the QW reverses sign, in which case the PL peak energy should red-shift again. These trends are in agreement with our experimental observations, where the QW emission FWHM decreased and the peak energy blue-shifted with decreasing GaN cap layer thickness (decreasing total electric field across the QW).

4. Conclusions

We have presented low temperature PL spectra from four single InGaN/GaN QW structures containing an *n*-type InGaN UL with different GaN cap layer thicknesses. The total electric field across the QW was predicted to decrease with decreasing cap layer thickness due to the decreasing range of the surface polarization field. The FWHM of the QW emission peak decreased with decreasing cap layer thickness (increasing total electric field) while, overall, the peak energy of the emission blue-shifted.

Atomistic tight-binding calculations were performed and repeated 40 times to simulate variations in the random InGaN alloy, featuring monolayer WWFs. An external electric field was applied to the simulated QWs with the strength varied to create cases which, in a continuum-based model, would be equivalent to the full internal electric field, a reduced internal field, "zero" internal field and one where the internal field is slightly reversed. The calculated potential isolines showed that large local variations occur in the electric field, meaning that a truly "zero" field QW cannot exist due to the alloy disorder and variations in the electric field stemming from structural inhomogeneities. The calculated hole ground state charge densities were found to be strongly localized by random alloy fluctuations for all values of total internal electric field. The electron ground state charge densities were found to be localized by a combination of the random alloy fluctuations and the WWFs, but the importance of the WWFs was found to be reduced as the total QW internal electric field is reduced towards zero. Calculations of the average

transition energy and its standard deviation showed that the former decreased with decreasing total internal field, due to the reduction of the QCSE, while the latter increased, due to the reduction in the variation in ground state transition energies. As these calculated parameters are analogous to the peak emission energies and FWHMs determined for the PL spectra, we can conclude that the trends observed in our theoretical model are in good agreement with the experimental work.

Acknowledgments

References

1) S. Schulz, M. A. Caro, C. Coughlan, and E. P. O'Reilly, Phys. Rev. B **91**, 035439 (2015).

2) D. S. P. Tanner, M. A. Caro, E. P. O'Reilly, and S. Schulz, RSC Adv. **6**, 64513 (2016).

3) D. Watson-Parris, M. J. Godfrey, P. Dawson, R. A. Oliver, M. J. Galtrey, M. J. Kappers, and C. J. Humphreys, Phys. Rev. B **83**, 115321 (2011).

4) Y.-H. Cho, G. H. Gainer, A. J. Fischer, J. J. Song, S. Keller, U. K. Mishra, and S. P. DenBaars, Appl. Phys. Lett. **73**, 1370 (1998).

5) H. Schömig, S. Halm, A. Forchel, G. Bacher, J. Off, and F. Scholz, Phys. Rev. Lett. **92**, 106802 (2004).

6) A. Morel, P. Lefebvre, S. Kalliakos, T. Taliercio, T. Bretagnon, and B. Gil, Phys. Rev. B **68**, 045331 (2003).

7) M. Filoche, M. Piccardo, Y.-R. Wu, C.-K. Li, C. Weisbuch, and S. Mayboroda, Phys. Rev. B **95**, 144204 (2017).

8) S. Chichibu, T. Azuhata, T. Sota, and S. Nakamura, Appl. Phys. Lett. **70**, 2822 (1997).

9) K.L. Teo, J. S. Colton, P. Y. Yu, E. R. Weber, M. F. Li, W. Liu, K. Uchida, H. Tokunaga, N. Akutsu, and K. Matsumoto, Appl. Phys. Lett. **73**, 1697 (1998).

10) J. Bai, T. Wang, and S. Sakai, J. Appl. Phys. **88**, 4729 (2000).

11) I. L. Krestnikov, N. N. Ledentsov, A. Hoffmann, D. Bimberg, A. V. Sakharov, W. V. Lundin, A. F. Tsatsul'nikov, A. S. Usikov, Z. I. Alferov, Y. G. Musikhin, and D. Gerthsen, Phys. Rev. B **66**, 155310 (2002).

12) M. J. Davies, S. Hammersley, F. C.-P. Massabuau, P. Dawson, R. A. Oliver, M. J. Kappers, and C. J. Humphreys, J. Appl. Phys. **119**, 055708 (2016).

13) G. M. Christian, S. Hammersley, M. J. Davies, P. Dawson, M. J. Kappers, F. C.-P. Massabuau, R. A. Oliver, and C. J. Humphreys, Phys. Status Solidi C **13**, 248 (2016).

14) M. J. Davies, P. Dawson, F. C.-P. Massabuau, R. A. Oliver, M. J. Kappers, and C. J. Humphreys, Appl. Phys. Lett. **105**, 092106 (2014).

15) M. J. Davies, P. Dawson, F. C.-P. Massabuau, A. Le Fol, R. A. Oliver, M. J. Kappers, and C. J. Humphreys, Phys. Status Solidi B **252**, 866 (2015).

16) V. Fiorentini, F. Bernardini, F. Della Sala, A. Di Carlo, and P. Lugli, Phys. Rev. B **60**, 8849 (1999).

17) O. Mayrock, H.-J. Wünsche, and F. Henneberger, Phys. Rev. B **62**, 16870 (2000).

18) C. Haller, J.-F. Carlin, G. Jacopin, W. Liu, D. Martin, R. Butté, and N. Grandjean, Appl. Phys. Lett. **113**, 111106 (2018).

19) J. Zhang, J. Yang, G. Simin, M. Shatalov, M. A. Khan, M. S. Shur, and R. Gaska, Appl. Phys. Lett. **77**, 2668 (2000).

20) J. Xu, M. F. Schubert, A. N. Noemaun, D. Zhu, J. K. Kim, E. F. Schubert, M. H. Kim, H. J. Chung, S. Yoon, C. Sone, and Y. Park, Appl. Phys. Lett. **94**, 011113 (2009).

21) N. G. Young, R. M. Farrell, S. Oh, M. Cantore, F. Wu, S. Nakamura, S. P. DenBaars, C. Weisbuch, and J. S. Speck, Appl. Phys. Lett. **108**, 061105 (2016).

22) M. Baranowski, Ł. Janicki, M. Gladysiewicz, M. Wełna, M. Latkowska, J. Misiewicz, Ł. Marona, D. Schiavon, P. Perlin, and R. Kudrawiec, Jpn. J. Appl. Phys. **57**, 020305 (2018).

23) S. Birner, T. Zibold, T. Andlauer, T. Kubis, M. Sabathil, A. Trellakis, and P. Vogl, IEEE Trans. Electron Devices **54**, 2137 (2007).

24) D. M. Graham, A. Soltani-Vala, P. Dawson, M. J. Godfrey, T. M. Smeeton, J. S. Barnard, M. J. Kappers, C. J. Humphreys, and E. J. Thrush, J. Appl. Phys. **97**, 103508 (2005).

25) M. A. Caro, S. Schulz, and E. P. O'Reilly, Phys. Rev. B **88**, 214103 (2013).

26) B. Monemar, P. P. Paskov, J. P. Bergman, G. Pozina, V. Darakchieva, M. Iwaya, S. Kamiyama, H. Amano, and I. Akasaki, MRS Internet J. Nitride Semicond. Res. **7**, e7 (2002).

27) T. M. Smeeton, M. J. Kappers, J. S. Barnard, M. E. Vickers, and C. J. Humphreys, Appl. Phys. Lett. **83**, 5419 (2003).

28) M. J. Galtrey, R. A. Oliver, M. J. Kappers, C. J. Humphreys, D. J. Stokes, P. H. Clifton, and A. Cerezo, Appl. Phys. Lett. **90**, 2005 (2007).

29) C. J. Humphreys, Philos. Mag. **87**, 1971 (2007).

30) M. A. Caro, S. Schulz, S. B. Healy, and E. P. O'Reilly, J. Appl. Phys. **109**, (2011).

31) R. Pecharromán-Gallego, P. Edwards, R. W. Martin, and I. M. Watson, Mater. Sci. Eng. B **93**, 94 (2002).

32) P. Dawson, S. Schulz, R. A. Oliver, M. J. Kappers, and C. J. Humphreys, J. Appl. Phys. **119**, 181505 (2016).

33) S. Marcinkevicius, K. M. Kelchner, L. Y. Kuritzky, S. Nakamura, S. P. DenBaars, and J. S. Speck, Appl. Phys. Lett. **103**, 111107 (2013).

34) S. Schulz, D. P. Tanner, E. P. O'Reilly, M. A. Caro, T. L. Martin, P. A. J. Bagot, M. P. Moody, F. Tang, J. T. Griffiths, F. Oehler, M. J. Kappers, R. A. Oliver, C. J. Humphreys, D. Sutherland, M. J. Davies, and P. Dawson, Phys. Rev. B **92**, 235419 (2015).

35) M. J. Galtrey, R. A. Oliver, M. J. Kappers, C. J. Humphreys, P. H. Clifton, D. Larson, D. W. Saxey, and A. Cerezo, J. Appl. Phys. **104**, 013524 (2008).

Figure Captions

Fig. 1. (Color online) Conduction and valence band profiles for the four as-grown single QW structures simulated using Nextnano3. The position axis is defined with the interface between the UL and the bottom GaN barrier at zero. Energies are defined relative to the Fermi level.

Fig. 2. (Color online) Normalized PL spectra for the four single QW structures with different GaN cap layer thicknesses.

Fig. 3. (Color online) PL peak emission energy (blue circles, dashed line) and FWHM (red squares, solid line) varying with GaN cap layer thickness.

Fig. 4. (Color online) Electrostatic built-in potential, V_p, for different slices through the supercell of an arbitrarily chosen microscopic configuration for a c-plane $In_{0.15}Ga_{0.85}N$/GaN quantum well of width, $L_w = 3$ nm. The potential is shown here in the x-z-plane where the z-axis is parallel to the wurtzite c-axis. The y-coordinate values increase from left to right. (a) Full internal field, meaning no external field is considered. (b) Results for the situation that an external field is applied that approximately halves the magnitude of the internal field. (c) Situation that the external field approximately cancels the internal, spontaneous and piezoelectric related field. Please note the different color scales. The dashed white lines indicate the well interfaces.

Fig. 5. (Color online) Isosurface plots of the electron and hole ground state charge densities for the configuration used in Fig. 4 for the built-in potential. Electron charge densities are depicted in red and hole charge densities in blue. The charge densities are plotted at 20% (light surface) and 40% (dark surface) of the respective maximum values. The different columns correspond to the different external field values discussed in Fig. 4.

Fig. 6. (Color online) Blue circles, dashed line: Calculated average transition energy as a function of the electric field across an InGaN/GaN QW with 15% In. Red squares, solid line: Standard deviation of the average transition energy of the same structure as a function

of the electric field. Averages were taken following calculations that were repeated 40 times (40 different microscopic configurations).
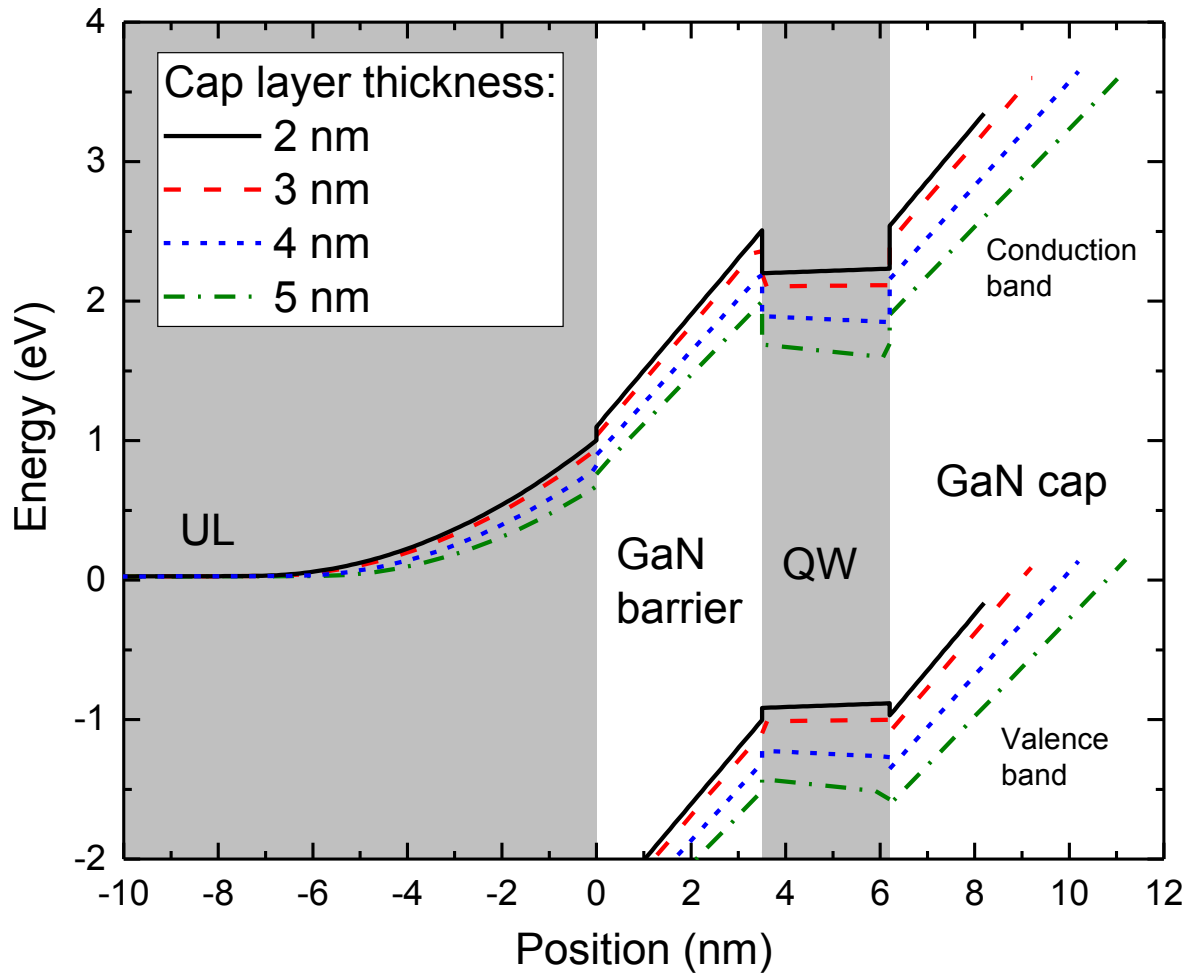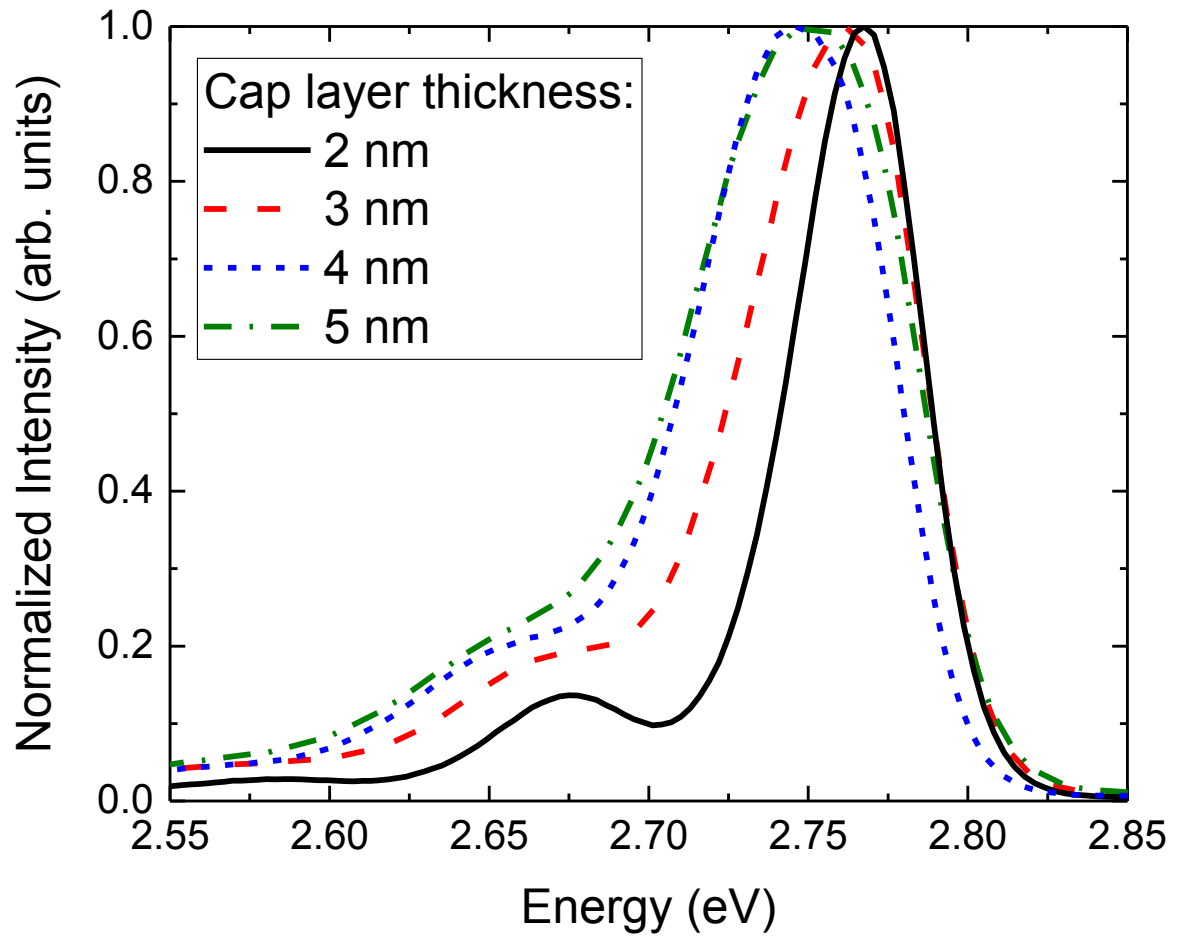
Fig. 1. (Color online)
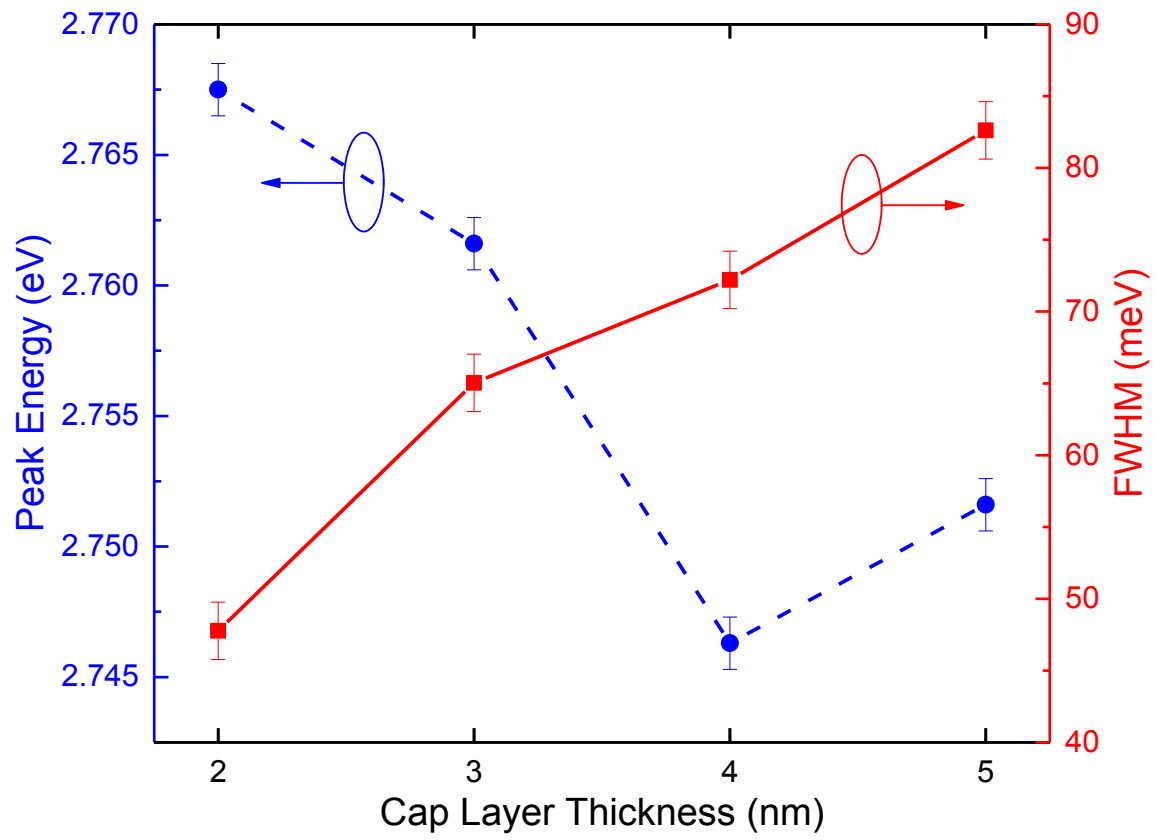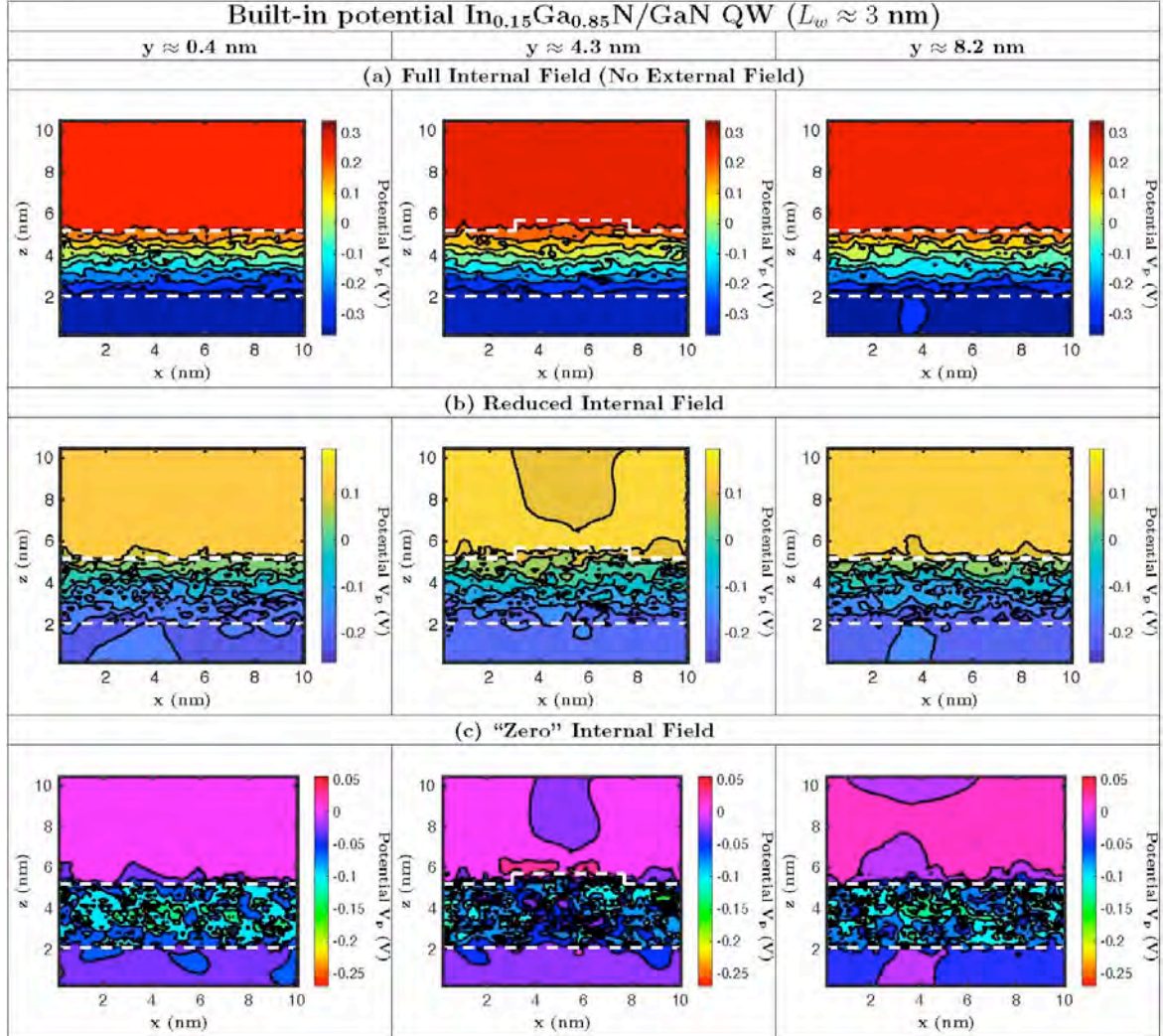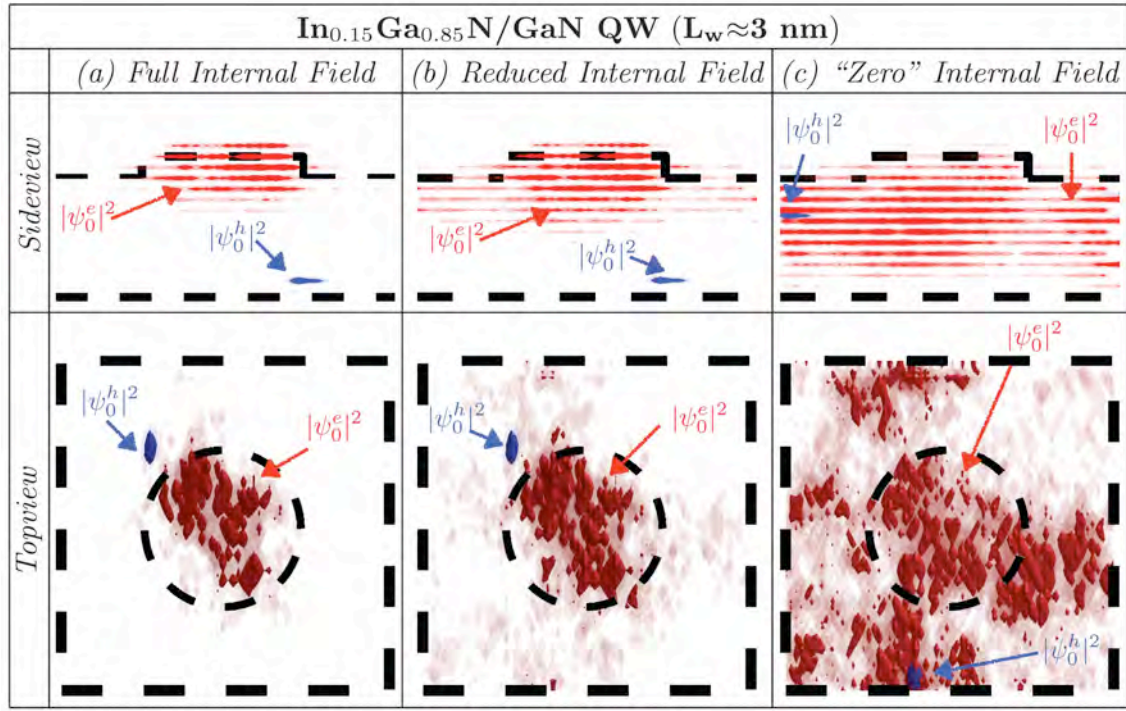
Fig. 2. (Color online)

Fig. 3. (Color Online)
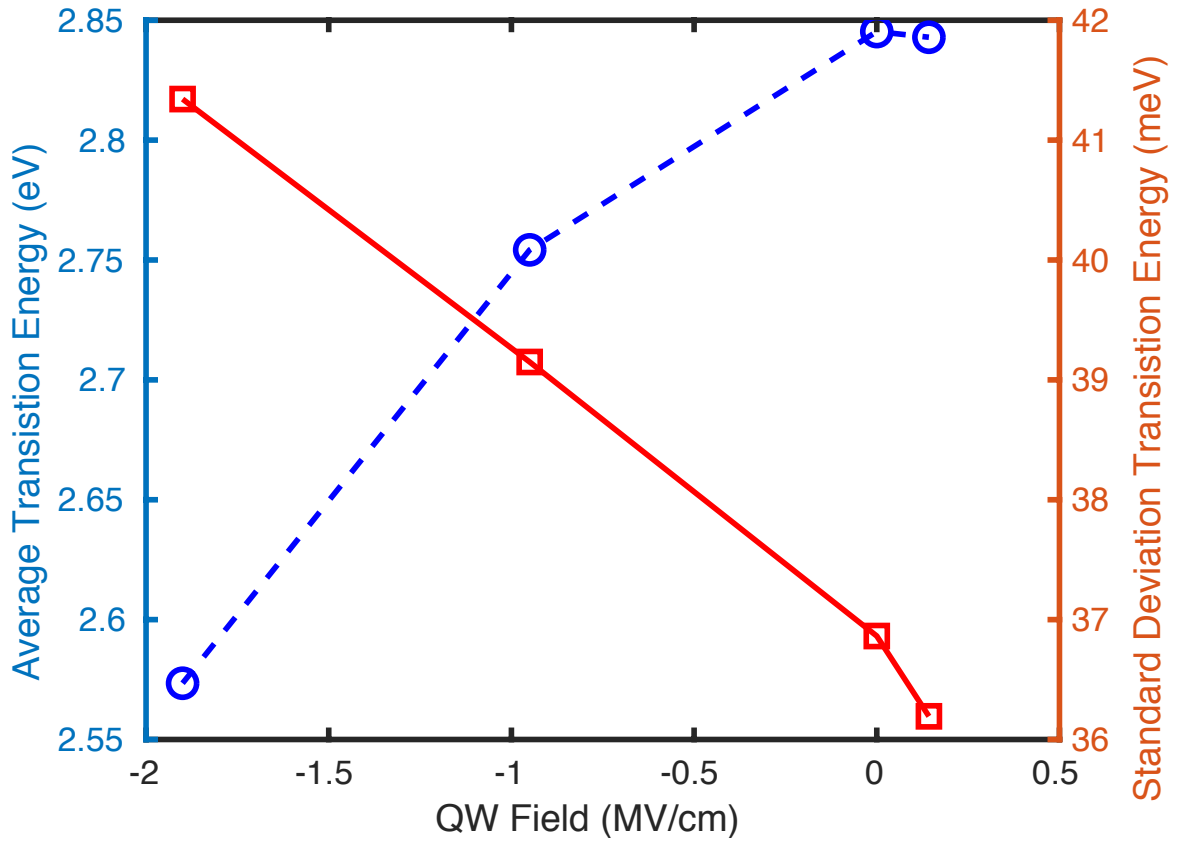
Fig. 4. (Color online)

Fig. 5. (Color online)

Fig. 6. (Color online)